Available on CMS information server

CMS CR -2020/169

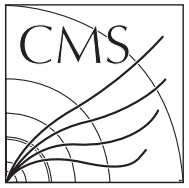

The Compact Muon Solenoid Experiment

Conference Report

Mailing address: CMS CERN, CH-1211 GENEVA 23, Switzerland

11 October 2020 (v3, 17 April 2023)

A Study of a Quartz Bar Detector in the Forward Region of the CMS Experiment at LHC

M. Khakzad, V. Samoylenko, J. Baechler, A. Baud, D. Druzhkin, B. Kaynak, R. Stefanovitch, M. J. Wagner, O. Atakisi, M. Kaya, S. Cerci, S. Ozkorucuklu, C. Simsek, D. Sunar Cerci, A. Mestvirishvili, A. Penzo

Abstract

In high rapidity regions of experiments at colliders (e.g. Large Hadron Collider LHC), along the direction of the interacting beams, the conditions are particularly challenging and the detectors need to have excellent time resolution, spatial resolution, high-rate capability and radiation resistance. Among various detector schemes proposed for these applications, combinations of Cherenkov radiators (quartz, sapphire, etc.) with fast photodetectors (e.g. Micro Channel Plate PMT (MCP PMT), Silicon PM (SiPM)) have been studied. Quartz-based calorimeters are already employed at CMS (Compact Muon Solenoid) experiment in the forward direction. Quartz bar array detectors were initially proposed as timing elements for the CT-PPS (CMS-TOTEM Precise Proton Spectrometer) project. We report here on the performance of one of these QUARTIC (QUARtz TIming Cherenkov) detectors, which was installed in 2018 (as test prototype) in the CMS Forward Zone near the CMS beam pipe.

Presented at *3rd International Iran-Turkey Joint Conference on LHC Physics*

A Study of a Quartz Bar Detector in the Forward Region of the CMS Experiment at LHC

M. Khakzad,[a] **V. Samoylenko,**[b] **J. Baechler,**[c] **A. Baud,**[c] **D. Druzhkin,**[c,1] **B. Kaynak,**[c,2] **R. Stefanovitch,**[c,3] **M. J. Wagner,**[c] **O. Atakisi,**[d,4] **M. Kaya,**[d,4] **S. Cerci,**[e,5] **S. Ozkorucuklu,**[e] **C. Simsek,**[e] **D. Sunar Cerci,**[e,5] **A. Mestvirishvili,**[f,6] **A. Penzo** [f]

[a] *Institute for Research in Fundamental Sciences (IPM), Tehran, Iran*
[b] *NRC-KI-IHEP, Protvino, Russia*
[c] *CERN, Geneva, Switzerland*
[d] *Bogazici University, Istanbul, Turkey*
[e] *Istanbul University, Istanbul, Turkey*
[f] *The University of Iowa, Iowa City, Iowa, USA*
[1] *Also at Tomsk State University, Tomsk, Russia*
[2] *Also at Istanbul University, Istanbul, Turkey*
[3] *Also at Belarusian State University, Belarus*
[4] *Also at Marmara University, Istanbul, Turkey*
[5] *Also at Adıyaman University, Adıyaman, Turkey*
[6] *Also at Georgian Technical University, Tbilisi, Georgia*

E-mail: suat.ozkorucuklu@istanbul.edu.tr

Abstract: In high rapidity regions of experiments at colliders (e.g. Large Hadron Collider - LHC) along the direction of the interacting beams, the conditions are particularly challenging and the detectors need to have high-rate capability, good radiation resistance, excellent timing and spatial resolution. Among various detector schemes proposed for these requirements, specific combinations of Cherenkov radiators (quartz, sapphire, etc.) with fast photodetectors (Micro-Channel Plate Photo-multiplier MCP-PMT, Silicon Photo-multiplier - SiPM) have been adequately studied. Some quartz-based calorimeters are hitherto employed at CMS (Compact Muon Solenoid) experiment in the Forward Region. Quartz bar array detectors were initially proposed as timing elements for the CMS TOTEM Precise Proton Spectrometer (CT-PPS) project. We report here on the instrumental performance of one of these QUARtz TIming Cherenkov - QUARTIC detectors, which was properly installed in 2018 (as test prototype called Forward Cherenkov Detector - FCD) in the CMS Forward zone near the CMS beam pipe.

Keywords: Cherenkov detectors; Timing detectors; Photon detectors for UV, visible and IR photons (solid-state) (Si-PMTs); Radiation-hard detectors

Contents

1 Introduction

At the High-Luminosity Large Hadron Collider (HL-LHC) era, an excellent timing precision will be genuinely needed to handle the severer pile-up conditions. A forward detector based on Cherenkov photons produced in quartz elements meets the requirements of superior time resolution [1, 2] and radiation resistance [3, 4] to survive and operate properly at the LHC beam conditions. In the CMS experiment, there are already three genuine types of forward detectors, namely calorimeters [5], and according to their eta coverage's

- Two HF (Hadron Forward) calorimeters [6], located at 11 m from the Interaction Point 5 (IP5), cover 3.0 $< |\eta| <$ 5.2
- One CASTOR (Centauro and Strange Object Research) calorimeter [7], located at 14-15 m from IP5, atthe minus end of CMS, covers -5.2 > η > -6.6
- Two ZDCs (Zero Degree Calorimeters) calorimeters for the Heavy Ion Run [8], located at 140 m from IP5, to detect very forward neutral particles at $|\eta|$ >8.0.

These three independent sets of forward detectors are based on either quartz fibers (HF and ZDC) or quartz plates (CASTOR) embedded in absorber blocks.

Furthermore, for detection of forward hadronic phenomena, in particular elastic pp scattering and diffractive processes, there is the TOTEM (TOTal Elastic and diffractive cross section Measurement) experiment [9] in the same intersection point of LHC (IP5) where CMS is located. The TOTEM experiment includes T1 and T2 tracker telescopes integrated into the CMS detector and Roman Pots (RPs) installed in the LHC tunnel.

- T1 and T2 are embedded in the forward parts of CMS on each side of the IP5. The η-coverage is $3.1< |\eta| <4.7$ for T1 and $5.3< |\eta| <6.5$ for T2. T1 and T2 enable charged particle tracking and trigger capabilities to the CMS experiment defining a fully inclusive trigger, including single and double diffraction.

- The Roman Pots (RPs) system consist of five stations placed in the LHC tunnel on the Long Straight Section (LSS5) site between 203 m and 220 m symmetrically on both sides of IP5. RPs are inserted inside the LHC beam pipe that can bring detectors to a few millimeters distance from the proton beam once it stabilizes. The entire RP system is a magnetic spectrometer using LHC magnets.

The combination of CMS and the TOTEM experiments (Fig. 1) gives an exceptionally large η-coverage[1] which is well suited for studies of a wide range of proton and nuclear interaction phenomena. To be specific, while the TOTEM data taking with RPs close to the circulating beams were usually limited to low intensity and high β^* runs, the implementation of new detectors in the RPs allowed high precision tracking and timing of diffracted protons (CT-PPS) [11]. At standard LHC luminosity, CT-PPS gives access to the study of exclusive production of central states, via photon and/or (multi-)gluon exchanges. There is a possibility of correlating the central states' properties measured in CMS with those tagged protons and of surveying a vast domain of diffractive masses.

2 Principle Scheme of Detector

The experimental challenges are essentially related to large pileup events, giving multiple pp interactions per bunch crossing, and detectors operating very close to the LHC beams under critical radiation levels: proton flux up to $5\times10^{15}\text{cm}^{-2}$ on the detectors and 100 Gy on the readout electronics at 100 fb^{-1} luminosity. The detectors should be radiation resistant and provide a precise Time-of-Flight (ToF) measurement of leading protons to help in reducing pileup effects by selecting the associated interaction primary vertex (time resolution of 10 ps corresponds to 2 mm of spatial resolution).

2.1 Cherenkov detectors

Detectors based on Cherenkov light produced in quartz (SiO_2) elements meet the requirements of excellent radiation resistance and optimal time resolution. In any radiator, Cherenkov photons are

[1] In addition, Forward Shower Counters (FSC) [10] made of scintillator paddles covering the non-instrumented region ($6< |\eta| <8$) were used between CASTOR and ZDC in 2015 with the role of detecting hadron production at large rapidity and tagging diffractive events.

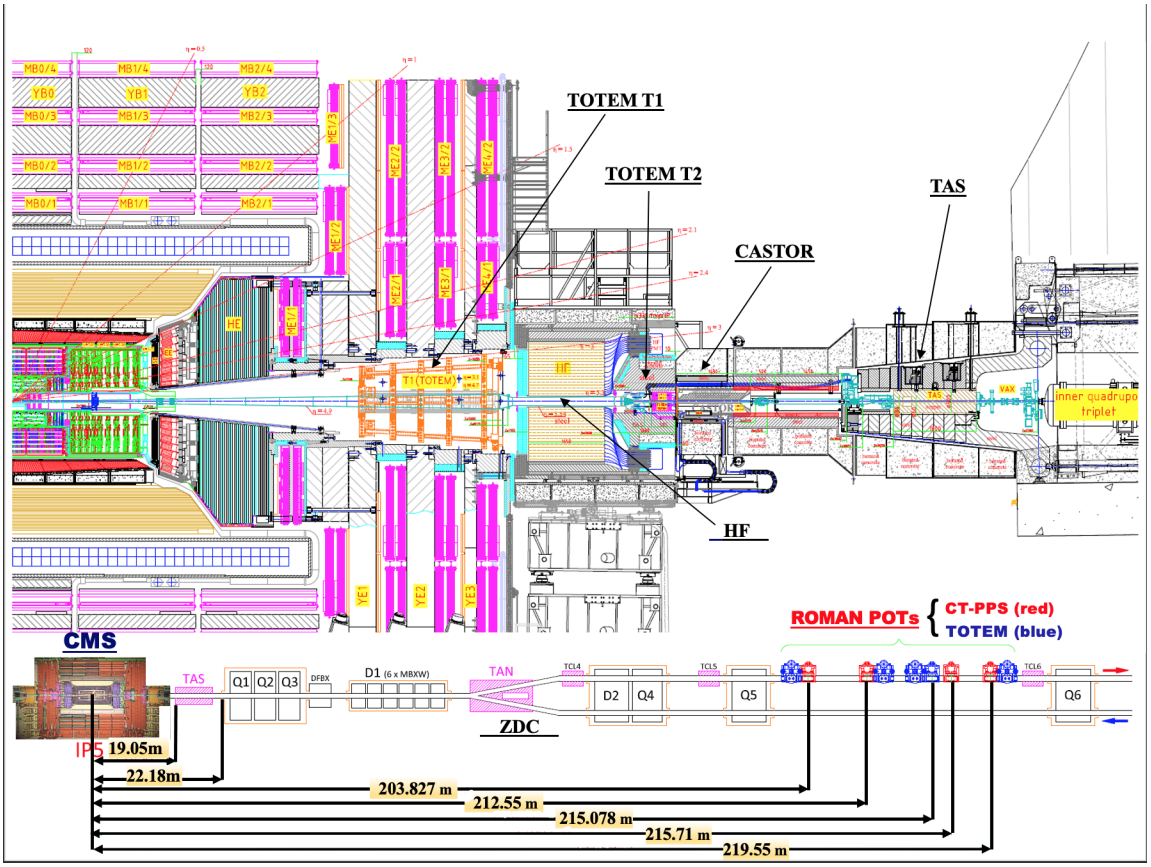

Figure 1. CMS Forward Region indicating Quartz Cherenkov calorimeters, CT-PPS and TOTEM detectors

emitted along the particle path in a cone with half angle θ_c given by $cos(\theta_c) = 1/n(\lambda)$ where $n(\lambda)$ is the refraction index, and λ the wavelength of emitted photons. The number of Cherenkov photons radiated is proportional to $1 - 1/n^2(\lambda)$ and for charge $Q = 1$ and $\beta = 1$ given as

$$\frac{d^2N}{dxd\lambda} = \frac{2\pi\alpha}{\lambda^2}\left(1 - \frac{1}{n^2(\lambda)}\right) \tag{2.1}$$

where α is the fine structure constant. When the particles are parallel to the radiator bar the Cherenkov light that hits the sides is completely reflected internally. The approximate rule for the number of photons in a typical detector can be calculated by $N_{ph} \approx 500\,\mathrm{cm}^{-1} L\,(\mathrm{cm})\, sin^2\theta_c$. For the Hamamatsu type S-10362-33 Multi Pixel Photon Counter (MPPC) [12] photodetector wavelength dependent parameters such as the refractive index, Cherenkov emission angle, light absorption length, and photon detection efficiency (PDE) are summarized in Table 1.

2.2 The QUARTIC concept

In the classic case of the in-line radiator and photodetector configuration, photodetector is naturally exposed to the energetic particles and may invariably suffer from radiation damage. However, by properly using longer bars, photodetectors can be kept sufficiently away from the high radiation regions. Two configurations of quartz bar Cherenkov detectors for timing (QUARTIC) were proposed:

Table 1. Properties of quartz bar and photon detection efficiency of a typical photodetectors as a function of wavelength

Wavelength	**Refraction Index**	**Cherenkov Emission Angle**	**Absorption Length**	**PDE** (%) **MPPC**
λ(nm)	$n(\lambda)$	θ_c(Degree)	$L_{abs}(\lambda)$(cm)	S-10362-33
250	1.510	48.5	95	0
300	1.488	47.8	104	5
350	1.475	47.3	111	38
400	1.470	47.1	120	48
450	1.465	47.0	122	50
500	1.462	46.8	125	47
550	1.460	46.8	128	40
600	1.458	46.7	130	30
650	1.456	46.6	130	24
700	1.455	46.6	130	18
750	1.450	46.4	130	13

- Angled-bars QUARTIC with MCP-PMTs readout, a baseline for ATLAS AFP [13]
- L-bar QUARTIC with SiPMs readout, the primary baseline for PPS [14]

In the first case, straight quartz bars are properly arranged at an Cherenkov opening angle with respect to the particle's direction to optimize direct transmission of emitted photons to reach the photodetector. In the second case, the bars are L-shaped with one arm aligned in the particle's direction, and the other (orthogonal) arm acting as a light-guide for photons to reach the photodetector. One critical point was the innovative production of L-shaped bars as single crystals with the required parameters and dimensions. Alpha-TM (a Russian company) produced L-bars with a precision better than 50 μm with optical surface polishing quality. Tests of surface quality were performed by Atomic Power Microscope in NIC "Kurchatov Institute" where the roughness of the surfaces measured on a 10 μm×10 μm square was better than 10 nm.

The quartz L-bar configuration had allowed to assemble a radiation hard 2D edge-less detector with the photodetector sufficiently away from the beam region. The construction and development of the first two QUARTICs with 20 L-bars each were carefully performed by CERN, IHEP and FNAL groups. The first QUARTIC-Q1 consisted of half quartz, half Sapphire where the second QUARTIC-Q2 consisted of all quartz were completed in 2015. The L-bar QUARTICs were intended to be inserted in Roman Pots or in Moving Beam Pipe (MBP) apparatus [15].

2.3 Early timing results of quartz detectors

In earlier studies on single quartz bar based Cherenkov detectors showed promising $\sigma_t \approx 16$ ps timing resolution results [16, 17]. Later, test beam studies on the "straight", "inclined" and "L-Bar" configurations were carefully performed at FNAL in 2012. A timing resolution of $\sigma_t \approx$ 30 ps were obtained reliably using a SiPM as photo-readout and these successful results were also

confirmed with an accurate Monte Carlo simulations [14]. The former and earlier timing resolutions measurement (σ_t) for the straight, inclined and L-Bars are succinctly summarized in Table 2.

Table 2. Earlier timing resolution measurement of straight, inclined and L-shaped bars

Radiator	**Configuration**	**Photodetector**	**DAQ**	σ_t (ps)	**Ref.**
Quartz 10 mm	Cylinders Ø 10 mm	Photonics 85011 MCP-PMT (10 μm)	ORTEC NIM+TAC+ADC 1 GHz BW	14	[16]
Quartz 30 mm	Straight bar in-line	HPK MPPC S10362-330050C 3600 pixels (50 μm)	DSR4 (5 GHz) WaveForm Digitizer	30	[14]
Quartz 80 mm	Inclined ($\theta_c \approx 48^0$) 6x6 mm^2	Photek PMT210 MCP-PMT (10 μm)	ORTEC NIM+TAC+ADC 1 GHz BW	16	[14]
Quartz 30 mm	L-Bar	HPK MPPC S10943-0035 3x3 mm^2	DSR4 (5 GHz) WaveForm Digitizer	32	[14]

A group of L-shaped quartz bars were acting as radiators for incident particles in one (horizontal) arm whereas the other (vertical) arm had the function of light guide attached to a SiPM photodetector as shown in the Fig. 2 (left). The full Q2 assembled by grouping 20 L-bars with different dimension to form a 5 × 4 array of horizontal bars, reaching the SiPM array through the vertical leg as shown in Fig. 2 (right).

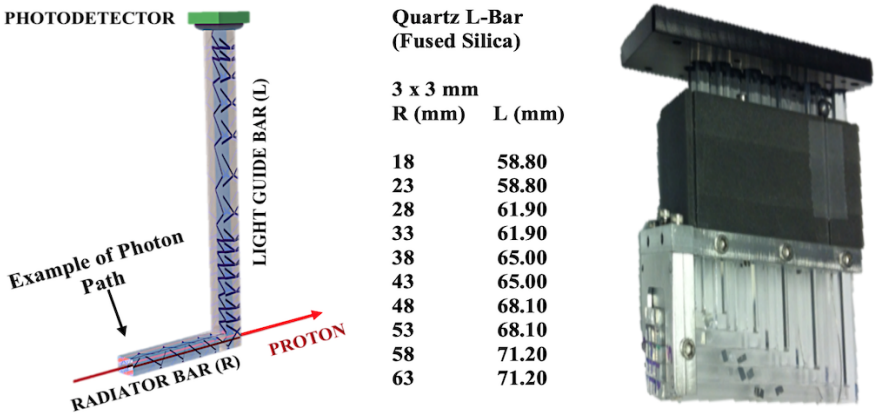

Figure 2. A simplified scheme of the L-Bar principle, and the dimensions of the L-bars used in the Q1/Q2 prototypes (left) and a picture of the QUARTIC assembly (right).

In 2015, beam tests were carefully performed with the full QUARTIC module assembly using SiPM as photodetector at CERN. The timing resolution with the NINO + HPTDC DAQ system

were typically $\sigma_t \approx 200$ ps (not corrected for the MCP-PMT reference counter contribution) and an accurate interpretation was really hard. On the other hand a $\sigma_t \approx 90$ ps timing resolution was allegedly obtained with a fast oscilloscope as the best result.

It is meaningful to analyze the altered the tests conditions in 2012 and in 2015 to clarify the significant variations in the results and possibly recover the original performances. The key differences between the 2012 test modules and the 2015 operational prototypes are listed in Table 3.

Table 3. Comparison of QUARTIC Setups in 2012 and 2015[2]

QUARTIC	**2012 Test Modules**	**2015 Prototype**
L-bar configuration	2 bars adjacent (1 side)	20 (4×5) bars adjacent (2, 3, 4 sides)
L-bar cross-section	3.0×3.0 mm^2 bars.	3.0×3.0 mm^2 bars
Separation	200 μm (2 wires)	2 adjacent side Al foils + glue spot
R-segment size	30.0 - 40.0 mm	18.0 - 63.0 mm
L-segment size	40.0 - 43.2 mm	58.8 - 71.2 mm
Manufacturer	Specialty Glass (US)	Alpha-TM (RU)
SiPM (Hamamatsu)	S10931-10362 MPPC	S-12572-050-P
Beam	120 GeV/c proton	180 GeV/c hadrons
Beam definition	2×2 mm^2 trigger counter.	Beam covers 4×5 bars area
Electronics	ORTEC VT120x20 Ampl.	Differential amplifier; NINO
Time resolution (σ_t)	30-35 ps	75-125 ps

With these contradictory results, the CT-PPS collaboration naturally decided to use Diamond detectors over the QUARTIC detectors in 2016. The diamond detectors utilize some possible advantages over the QUARTIC concerning their practical use in RPs, less material budget close to the beam and higher pixel segmentation.

2.4 Early test beam activities on the QUARTIC

The main purpose of the QUARTIC modules was to measure the time-of-flight of the small angle scattered protons with precision of the order of 10 ps, in order to determine the interaction point from where they came with precision of about 1 mm.

The QUARTIC modules were installed at the H8 test beam at CERN in 2015 and carefully tested. The SiPMs used as photodetectors were Hamamatsu MPPC model S-12572-050-P with a (3.0×3.0mm^2) sensitive area which precisely matched the L-bars cross-section. The L-bars were carefully stacked with a minimum spacing to adequately prevent light losses and cross-talk. However, a large number of signals sharing have been observed across the multiple bars and of a time resolution of 75 - 125 ps achieved in 2015 compared to 30 - 35 ps obtained with a single L-bar in 2012 [18]. Another source of uncertainty in the 2015 results was associated with the time reference signal from a MCP-PMT installed in the beam line to provide a precise time reference for the QUARTIC channels. The beam was crossing the face of the MCP-PMT through the front photo-cathode window, and producing Cherenkov photon pulses there (such a system had been

[1]Courtesy of M. G. Albrow; private communication

calibrated earlier, providing timing precision close to 10 ps) however, such a resolution could not be calibrated “in situ” during the 2015 run and might have an impact on the deterioration of the time resolution with respect to earlier results.

Similar test were carried out in 2017, providing a time resolution of 60 - 100 ps with MCP-PMT and was used as a time reference during the 2018 Q2 test beam in H8. Unfortunately, only one of the MCP-PMTs were operating during that time and therefore the time reference counter was not self-calibrating (i.e. continuously calibrated independently from the Q2 channels).

2.5 Recent QUARTIC test beam studies

The QUARTIC-Q2 module used in 2018 consisted of all quartz bar arrays, with the SiPM matrix attached to the light guides of the quartz bars with a coaxial cable adaptor to readout the SiPM (positive) signals. During 2018 test beam with the Q2 module at H8, the 2015 test beam setup was used in order to find the uncertainties on the time resolution.

The Q2 module was refurbished at IPM-Tehran and equipped with a SiPM voltage distribution board. The SiPM bias voltage typically was set to -68 V. A LED pulser system was optionally added to the Q2 module as a diagnostic system and used for illuminating the front face of the L-bar array, to study carefully the transmission efficiency and SiPM response, including mapping of the bars and cross-talk. At CERN, a defining scintillator counter of size $15 \times 12 \times 2$ mm^3 installed behind the L-bar array and readout with an MPPC S10931-050P.

The QUARTIC-Q2 was tested in the H8 area with a beam momentum 180 GeV/c tuned for negative hadrons. The measurements carried out with three different trigger (TR) settings ("Narrow", "Wide" and "Self") at 2 - 3 mV threshold level utilizing S1 (12×15 mm^2), DM1, DM2 and S2 (30×30 mm^2) beam defining counters as shown in Fig.3. The narrow trigger required N = S1 · S2 · DM1 · DM2, wide trigger required W = S2 · DM1 · DM2 and a self trigger required on active channel of Q2.

The test beam setup was also supplemented with a counter consisting of two MCP-PMTs facing directly a straight quartz bar orthogonal to the beam direction. The SiPM pulses obtained with the

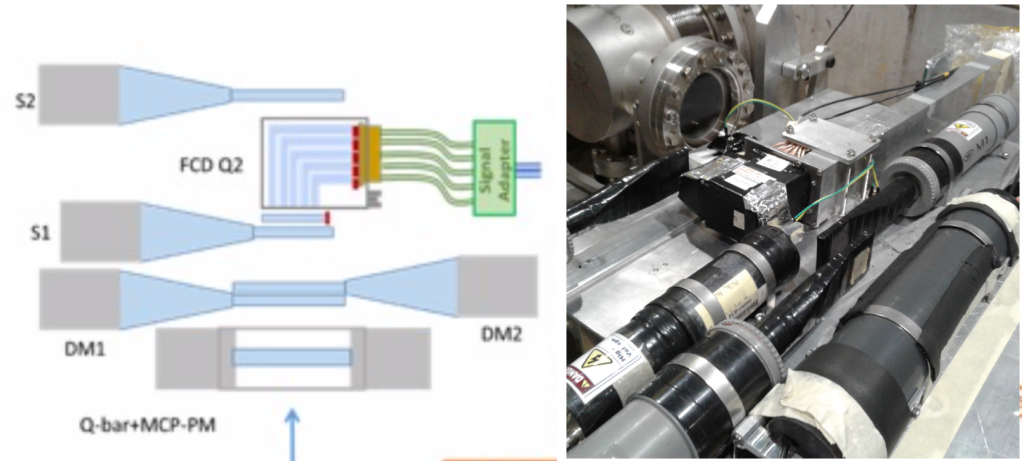

Figure 3. Left: Sketch of the setup at H8 test beam with Q2 module and trigger counters; Right: Photo of the setup mounted on a scanning table in H8.

Agilent Digital Signal Oscilloscope (DSO) [19] show a clustering structure (Fig. 4) proportional to number of hit pixels ($\approx N_{phe}$) which corresponds to charge distribution of few pC (Fig. 5). These results were agreed with GEANT [20] simulations estimation of Cherenkov photons emission, transmission in quartz and conversion in the SiPMs.

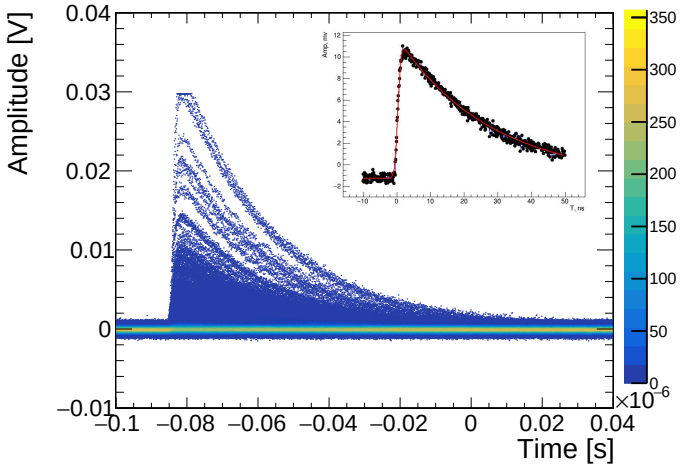

Figure 4. The SiPM pulses and corresponding charge distribution with fitted function (2.2) (red line)

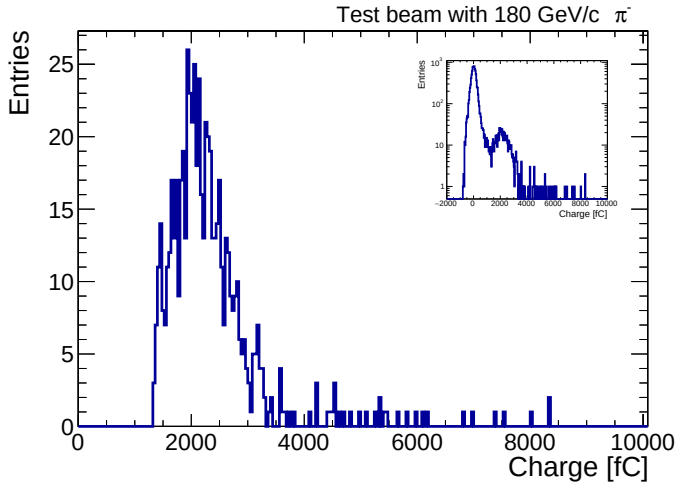

Figure 5. Pedestal-subtracted charge distribution of a Q2 channel and the distribution before pedestal subtractions (the insert) for 180 GeV/c negative π beam.

The SiPM signals can be ideally fitted by a function [21]

$$f(t) = A\frac{e^{(t-t_0)/\tau_d}}{1+e^{(t-t_0)/\tau_r}} + p \tag{2.2}$$

where A represents the amplitude of the proper signal, τ_d and τ_r are decay and rise times, t_0 is the time corresponding to half of the amplitude and p is the pedestal value (base line shift). The five parameter fit function adequately describes the data (Fig. 4 insert). The rise and the decay times

were typically ≈ 0.5 ns and ≈ 30 ns, respectively. Only a specific group of L-bars were measured with the DSO, concentrating around a certain region and neighboring channels, in order to estimate also the possible cross-talk effects. Some of the runs allowed to simultaneous extraction of the time resolution of three separate channels as illustrated in Fig. 6.

DSO Channels	Quartic Channels
Channel 1	2
Channel 2	7
Channel 3	12
Channel 4	MCP

Figure 6. The QUARTIC-Q2 channels mapping and DSO channels used for data taking in H8.

The time differences obtained with N (narrow) trigger between the MCP reference (DSO channel #4) and two Q2 channels #2 and #7 (DSO channels #1 and #2) are shown in Fig. 7 and

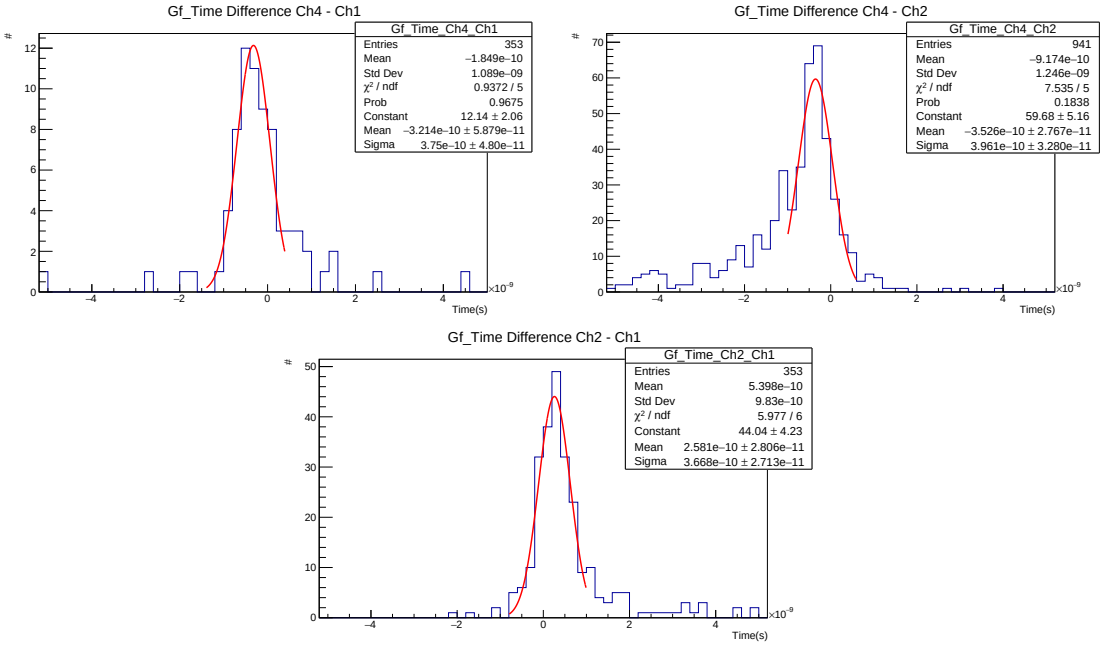

Figure 7. Time difference distributions between MCP and two Q2 channels

extracted time differences between the MCP reference counter and two other SiPM Q2 channels are listed in Table 4.

An extensive amount of care has to be taken to choose the time (pick-off) marker since a proper part of the signals directly correlated with the passage of the particle from detectors (typically a well-defined position of the signal rise time). While the precise determination of time of flight (ToF) requires, in general, accurate calibrations of the detector response, intrinsic delay, etc., the

Table 4. Time distribution values between MCP and two Q2 channels

DSO ch.	Q2 time resolution (ns)
4-1	0.3750 ± 0.0480
4-2	0.3960 ± 0.0328
1-2	0.3360 ± 0.0271

precision in the measurement of the time delay between the signals of the two detectors can be properly obtained from the standard analysis of the statistical distribution of T = t_2 - t_1; if the T distribution is adequately represented by a Gaussian, with mean value of T_M and standard deviation of σ_T, the precision in ToF can be associated with σ_T. This quantity refers to a pair of detectors (D_1 and D_2); it has become customary to consider as the "intrinsic" time resolution for an individual detector assuming that D_1 and D_2 have resolutions of σ_1 and σ_2, respectively. With the hypothesis that the D_1 and D_2 measurements are independent (no co-variance), the standard deviation of T can be calculated from $\sigma_T^2 = (\sigma_1^2 + \sigma_2^2)$. From the measurement of σ_T, it would not be possible to extract σ_1 and/or σ_2. If the two detectors D_1 and D_2 considered to be identical ($\sigma_1 = \sigma_2 = \sigma$) then $\sigma_T = \sqrt{2}\sigma$ can be assumed. This is often the way in which the resolution of individual counters is determined, but it is not immune from confusion and possible errors.

On the other hand with three counters (D_1, D_2 and D_3), their "intrinsic" time resolutions σ_1, σ_2 and σ_3 can be extracted from the respective times ($T_{21} = t_2 - t_1$), ($T_{31} = t_3 - t_1$) and ($T_{32} = t_3 - t_2$). The three counters' scheme introduces various constraints to the ToF measurement:

$$T_{21} + T_{32} = T_{31} \; ; \; \sigma_{21}^2 = (\sigma_2^2 + \sigma_1^2), \; \sigma_{31}^2 = (\sigma_3^2 + \sigma_1^2) \text{ and } \sigma_{32}^2 = (\sigma_3^2 + \sigma_2^2). \tag{2.3}$$

The resolutions of the three counters can be obtained from the "Pythagorean" relations above:

$$2\sigma_1^2 = \sigma_{21}^2 + \sigma_{31}^2 - \sigma_{32}^2 \; ; \; 2\sigma_2^2 = \sigma_{21}^2 + \sigma_{32}^2 - \sigma_{31}^2 \; ; \; 2\sigma_3^2 = \sigma_{31}^2 + \sigma_{32}^2 - \sigma_{21}^2 \tag{2.4}$$

In the specific case of the H8 results for Q2, the standard deviations extracted from Fig. 7 with reference to the DSO channel were $\sigma_{41} = 0.375 \pm 0.048$ ns, $\sigma_{42} = 0.396 \pm 0.033$ ns and $\sigma_{12} = 0.367 \pm 0.027$ ns giving the time resolutions of $\sigma_1 = 0.242 \pm 0.020$ ns, $\sigma_2 = 0.274 \pm 0.030$ ns, $\sigma_4 = 0.286 \pm 0.020$ ns.

As explained before, the time pick-off marker is generally chosen as the point corresponding to the 50 % of the signal maximum amplitude, using a linear fit to the front of the signal (for instance between 20 % and 80 % of the maximum signal amplitude). The results above are obtained with this procedure. There are however theoretical (and experimental) criteria suggesting to use a different time pick-off, corresponding to a lower fraction (20 -30 %) of the signal maximum amplitude [22].

In Figure 8 the same signals have been linearly fitted in the range 10 % to 70 % and 30 % time pick-off point has been used to calculate the ToF resolution. As it can be appreciated in Fig. 8, $\sigma_{41} = 0.188 \pm 0.040$ ns, $\sigma_{42} = 0.231 \pm 0.017$ ns and $\sigma_{12} = 0.261 \pm 0.014$ ns; giving: $\sigma_1 = 0.169 \pm 0.020$ ns, $\sigma_2 = 0.216 \pm 0.020$ ns, $\sigma_4 = 0.082 \pm 0.020$ ns. These results seem to confirm the criteria given above and may be generalized to other cases where $\sigma_{41} = 0.375 \pm 0.048$ ns,

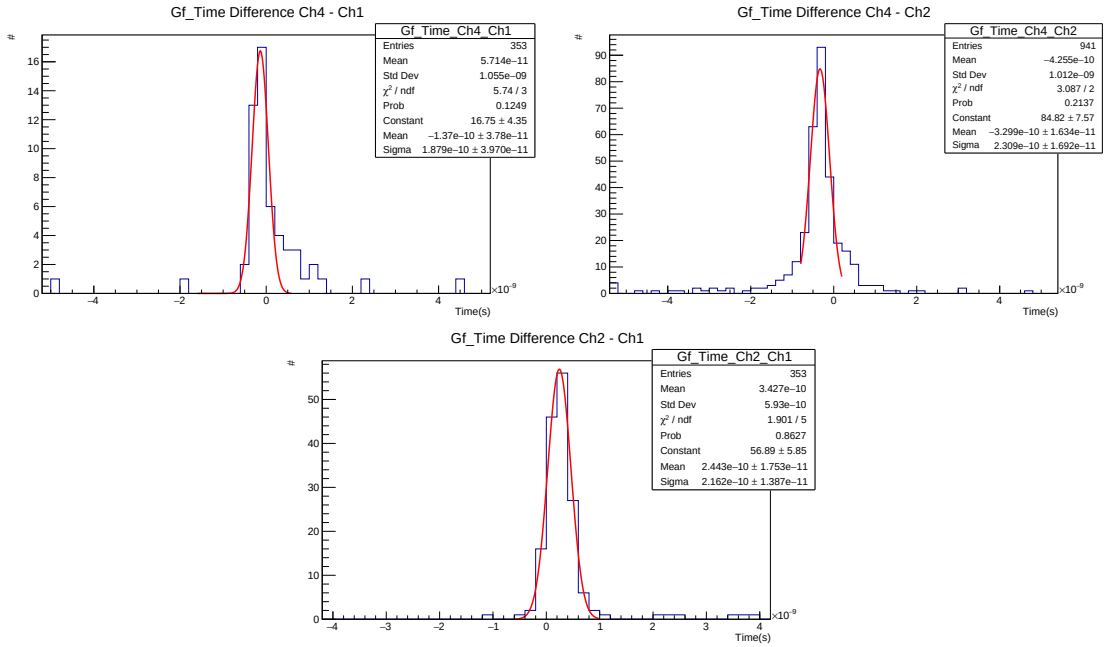

Figure 8. The time differences measured using a (linear) fit between 10 % and 70 %, and a time pick-off at 30 % of maximum amplitude.

$\sigma_{42} = 0.396 \pm 0.033$ ns and $\sigma_{12} = 0.367 \pm 0.027$ ns; giving the time resolution of $\sigma_1 = 0.242 \pm 0.020$ ns, $\sigma_2 = 0.274 \pm 0.030$ ns, $\sigma_4 = 0.286 \pm 0.020$ ns.

As a confirmation of the results above, other runs containing the same group of adjacent L-bars (#2, #7, #12), with internal trigger on one of them (#7) gives distribution of time differences as shown in Fig. 9. While the presence of time correlated signals in L-bar #7 and the MCP are obvious, with $\sigma_{23} = 0.127 \pm 0.007$ ns, $\sigma_{24} = 0.118 \pm 0.002$ ns and $\sigma_{34} = 0.134 \pm 0.012$ ns one can obtain results of $\sigma_2 = 0.079 \pm 0.010$ ns, $\sigma_3 = 0.100 \pm 0.040$ ns, $\sigma_4 = 0.089 \pm 0.030$ ns.

The sharp coincidence of L-bars #7 and #12 (and #2 in Fig. 8) is indicative of a significant degree of cross-talk between adjacent channels, e.g. due to beam particles crossing the periphery of two (or more) L-bars, either in the radiator parts or in the light-guides. Another possibility corresponds to optical cross-talk between adjacent or distant L-bars, due to photons escaping from one bar, and reaching others. There is no special optical shielding between L-bars, mainly relying on total internal reflection to contain the Cherenkov photons in the L-bar where they are produced. Depending on the surface quality of the bars, this may not be sufficient.

The results of 2018 H8 test beam studies indicate that with appropriate signal selection and time pick-off procedures, resolutions around 200 ps can be obtained for the Q2 L-bars, with respect to an external time reference (MCP + straight bar). Occasionally adjacent L-bars display signals in sharp coincidence indicating a significant degree of cross-talk. Some of these results are in line with the observations in the 2015 test beam runs. With $\sigma_{23} = 0.1275 \pm 0.0066$, $\sigma_{24} = 0.1185 \pm 0.0015$ and $\sigma_{34} = 0.1340 \pm 0.012$ one can obtain results of $\sigma_2 = 0.0786 \pm 0.0100$ ns, $\sigma_3 = 0.1004 \pm 0.0400$ ns and $\sigma_4 = 0.0887 \pm 0.0300$ ns. The results from two sets of runs in 2018 are summarized in Table 5.

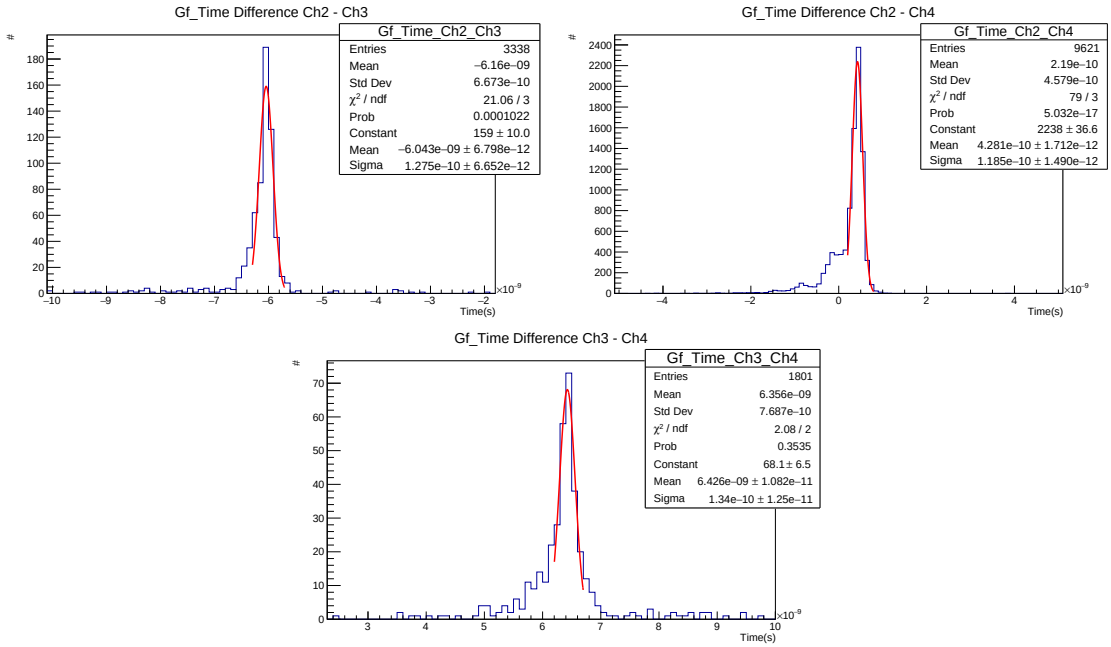

Figure 9. Time differences between three Q2 channels, triggering on one of them.

Table 5. Recent time resolution results of Q2 from H8 test beam.

DSO Chnl.	**QUARTIC Q2 Chnl.**	**Trigger (N) [(DM1*DM2)*S1*S2]**	**Trigger (S) [(#7) > 3 mV]**
1	# 2	σ_2 = 169 (±20) ps	
2	# 7	σ_7 = 216 (±20) ps.	σ_7 = 79 (±10) ps
3	# 12		σ_{12} = 100 (±40) ps
4	MCP	σ_{MCP} = 82 (±20) ps	σ_{MCP} = 89 (±30) ps

The straight quartz bar with MCP gives a time resolution of 60 - 80 ps with the bar orthogonal to the beam line. From a previous study, the response as a function of the bar inclination with respect to the beam line, the resolution at 45°reported to be about 20 ps.

In summary, the 2018 test beam runs of Q2 at H8 confirm the results obtained in 2015 [18] in a completely independent way. Another similarity with 2015 results is that the Q2 channels studied in 2018 show a non-negligible level of cross-talk, which appears also in charge correlations of (adjacent) Q2 channels (#2, #7, #12) as shown in Fig. 10; even eliminating pedestals, the three channels have significant correlations that might indicate cross-talk processes.

The timing resolutions for the three channels, summarized in Table 5, together with the MCP reference counter, correspond to values around 200 ps for the Q2 channels, and about 80 ps for the MCP reference counter. These results have been obtained with different L-bars and SiPMs, different triggering conditions and slightly different operating bias voltage values for the SiPM, showing a certain stability regarding the operating parameters. The intrinsic resolutions obtained

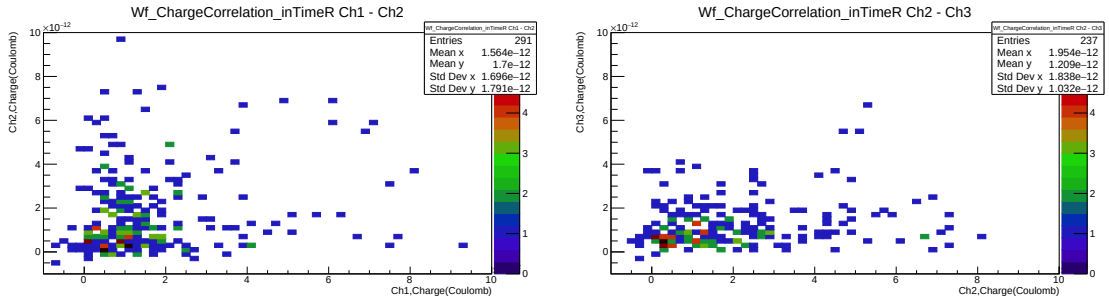

Figure 10. A 2-dimensional map of the (simultaneous) signals in the 3 (adjacent) Q2 channels, corresponding to L-bars #2, #7 and #12 (DSO Ch. 1, 2, 3 respectively)

here result from evaluations based on hypothesis of uncorrelated timing channels: in the opposite case, the extraction of intrinsic resolutions need to take into account covariance terms that may alter considerably the resolutions listed above.

3 Forward Cherenkov Detector Studies

In the operational perspective of running at higher LHC luminosity, the fundamental issue of high radiation resistance becomes more crucial for various active components of forward detectors and the quartz-based device option becomes more attractive, and probably necessary. In view of this renewed interest for quartz-based detectors in forward regions at LHC, we engaged in a comprehensive R&D program to extend and revisit previous work to correctly identify, document and test the essential properties of various possible configurations of quartz detectors and various photodetectors (MCP-PMT and SiPM). To adequately distinguish the intended goals of the previous QUARTIC project from the general targets of the present R&D program, the latter was called Forward Cherenkov Detectors (FCD) project. This multi-purpose R&D program is aiming at establishing sensitive timing detectors based on quartz radiators with appropriate photodetectors to be installed in proximity of the LHC beam pipes, where radiation resistance and optimal timing resolution in the range of 20 - 30 ps are required in order to properly distinguishing vertices at IP5 belonging to different (pile-up) events.

Therefore, one of the QUARTIC modules (Q2), was properly installed near the LHC beam pipe close to the CMS during the period of 13 TeV pp collisions in 2018 at LHC. We report here on the satisfactory results properly obtained during these full-scale tests.

3.1 Installation of FCD in CMS

The FCD module was installed as a demonstrator on the CASTOR table in 2018 during the technical stop (TS2) period[3]. The Q2 assembly was inserted through a vertical slot in the CASTOR table on the Collar platform at the negative rapidity end of CMS, as shown in Fig. 11 which is not necessarily to scale. The trigger defining scintillator, centered on the quartz bars' array, has dimensions (xy) of 15 × 12 mm^2 and thickness of 2 mm and is read out with a MPPC (3× 3 mm^2) in the center. The mean inclination of a track reaching the Q2 quartz radiator array is approximately 5 - 6 mrad,

[3]With agreement of CMS Technical Coordination, HCAL management and the CMS Executive Board

and is therefore crossing an appreciable thickness of the beam pipe, with a sizeable probability of showering.

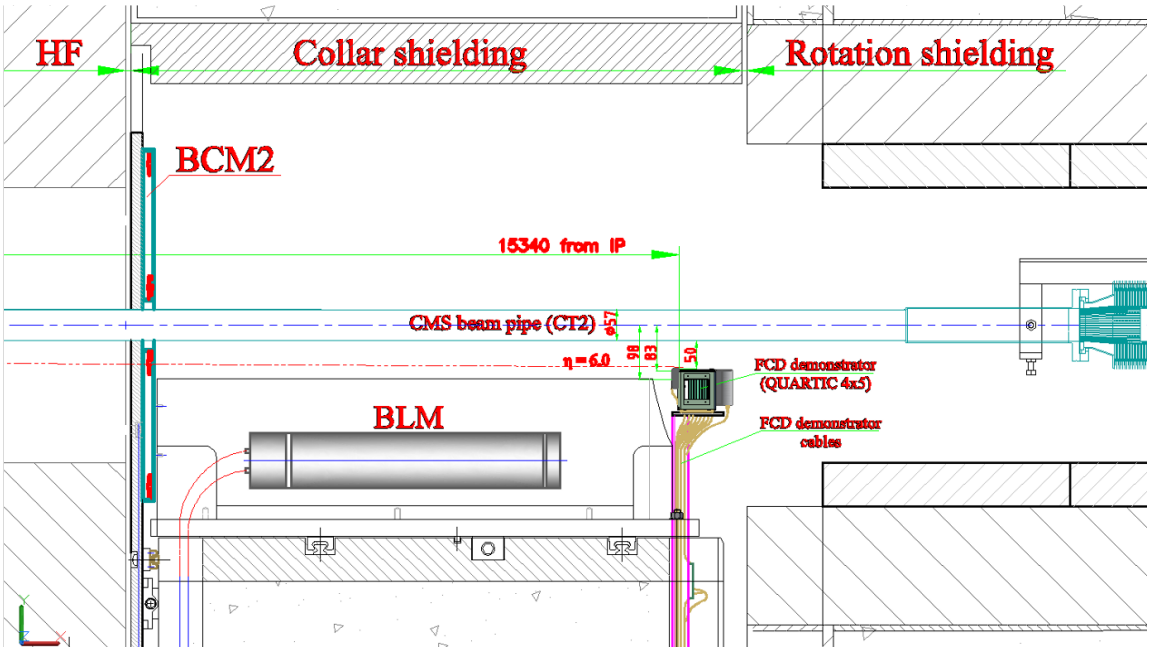

Figure 11. The geometry of FCD-PD installation with respect to IP5

3.2 Connecting FCD to the HCAL readout systems

The readout was performed by charge integration and encoding units (QIEs) and the data were stored in raw data format. The QIE10 is the latest device in a family of fast, wide dynamic range, dead-time-less ADCs developed for use in high-energy physics experiments [23, 24]. The QIE10 differs from previous generation chips by incorporating TDC information in the digital output.

The FCD readout was performed with the HF QIE-10 system. The configuration of the FCD module with connections to a stabilized LV power supply, a pulse inverter stage based on fast transformer cores, and to the HFM QIE10 readout system is shown in the Figure 12. The SiPM outputs were connected to the QIE10 system via an inverting transformer board, in order to feed the QIE10 inputs with negative polarity pulses. The QIE10 channel was read out in 10 time slices of 25 ns each. The data acquisition system is described in detail in [25].

The readout scheme for the Q2 module had been tested preliminary at the B904 QIE10 test facility and found to be compatible with CMS. A LED/Laser signal was fed to the Q2 module (illuminating the L-bars from the back side). The inverted Q2 SiPM signals were fed to QIE cables, reaching the QIE test modules. The same type of connection was implemented at UXC on the HF-QIE system, and it was tested with the HF- Laser calibration system.

3.3 FCD data taking with CMS

Under the supervision of the HCAL Operations Team, the FCD was included in CMS HCAL data taking stream as the HF-part described in the Seciton 3.2. Subsequently the module was readout

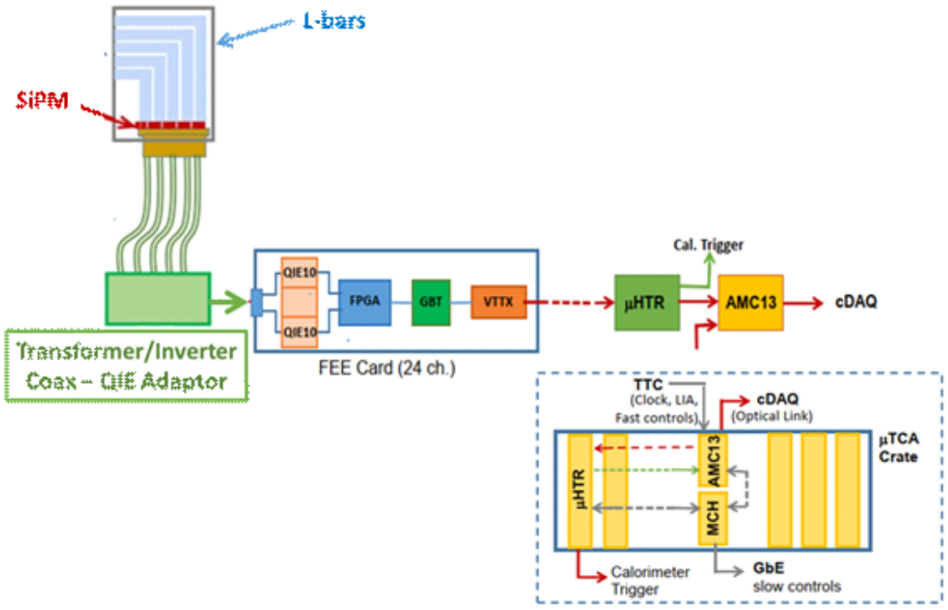

Figure 12. The schematic of FCD readout system

together with the HF-system during the initial phase of data taking after TS2. Calibration runs with laser were taken before, in order to confirm that FCD was giving signals acceptable from the HF–QIE10 with proper timing (only 6 Time Slices (TS) were used for FCD). In subsequent runs, data taking was performed with FCD at luminosity of $5\times10^{27} - 10^{28}$ cm^{-2} s^{-1} and accumulated about 36 M events, which have been analyzed to study the behaviour of the FCD channels. Here results obtained from a sub-sample of these runs are described, mainly with reference to "collisions" and "circulating beam", respectively. Comparing the two types of runs allows CMS to extract the genuine signals of particles produced in 13 TeV pp interactions, eliminating background contributions.

3.4 FCD Data analysis

All the results presented in this chapter are based on the standard CMS software framework (CMSSW). The collision data samples have been processed using current CMSSW during the year of data-taking and the standard reconstruction framework. The raw data distributions from the QIE10 readout are shown as a function of linearized ADC (charge) collected per 25 ns time slices (TS) for one of the FCD channels (Ch.10) in Fig. 13 (left). The FCD signals are typically concentrated in time slices 2 to 5; time slices 0 - 1 represent the pedestal level. In order to subtract the pedestal from the signal, the average of linearized ADC counts in the first two time slices were taken [i.e., (TS0 [Lin.ADC]+ TS1 [Lin.ADC])/2]. This average value is called as "pedestal charge" which is subtracted from the linearized ADC in each time slices for each event. The distribution of subtracted linear ADC as a function of time slices is shown in Fig. 13 (right).

The sum of linearized ADC in time slices from time slices 2 to 5 is shown before (Fig. 14 left) and after the pedestal subtraction (Fig. 14 right). After subtraction, the pedestal level estimated from TS 0 - 1, the FCD charge distribution still seems to have a residual pedestal peak as seen in Fig. 14 (right).

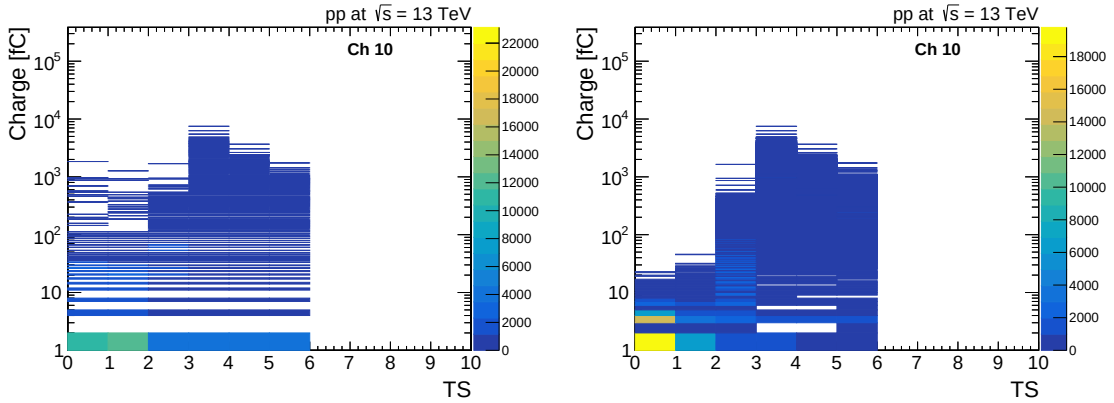

Figure 13. Linearized ADC charge vs TS shown before (left) and after the pedestal subtraction (right).

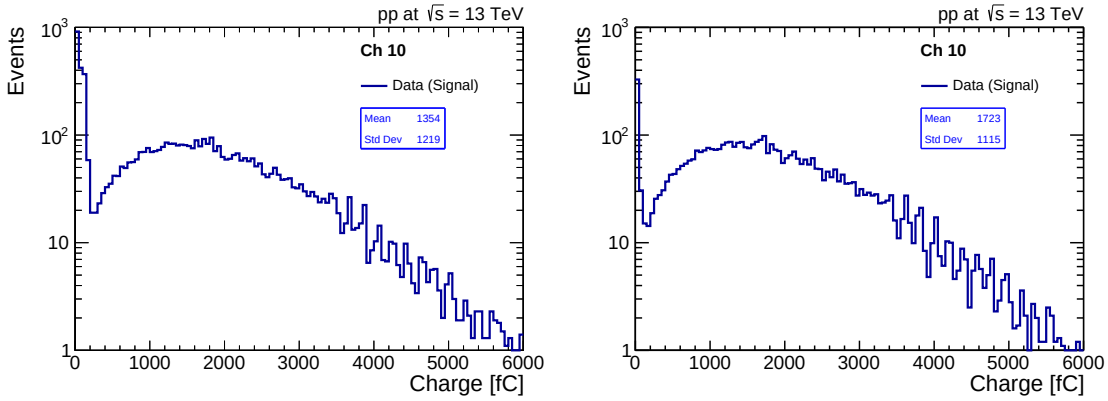

Figure 14. Charge distribution of one FCD channel readout in QIE10 shown before (left) and after (right) the pedestal subtraction.

The residual background in the distribution is eliminated by using non-interacting from circulating beam runs events represented by the red lines as shown in the Figure 15 (left); the blue lines corresponds to the response of one FCD channel in collision runs. In Fig. 15 (right), the charge distribution of one FCD channel after the pedestal subtraction and residual background elimination is plotted in linear scale. Typically the charge collected in one of the QIE channel corresponds to few fC, in agreement with estimations based on the amount of Cherenkov photons produced in the radiators and transmitted to the photodetectors, including their PDE and gain.

The Q2 module used as FCD was equipped with a 2 mm thick scintillator tile. This scintillator should therefore give a signal whenever a charged particle enters any of the FCD bars, therefore is called triggering scintillator. The charge distribution of trigger scintillator after the pedestal subtraction and residual background elimination (blue) is shown in Fig. 16 (left). The background from non-interacting beam events (red) are also shown in the same plot. The charge correlation of the one FCD channel with respect to the triggering scintillator shown in Fig. 16 (right). The charge correlations between different channels of the FCD module are also shown in lower half of the Figure 16.

The mean values and standard deviation (STD) of the charge distributions for all FCD channel

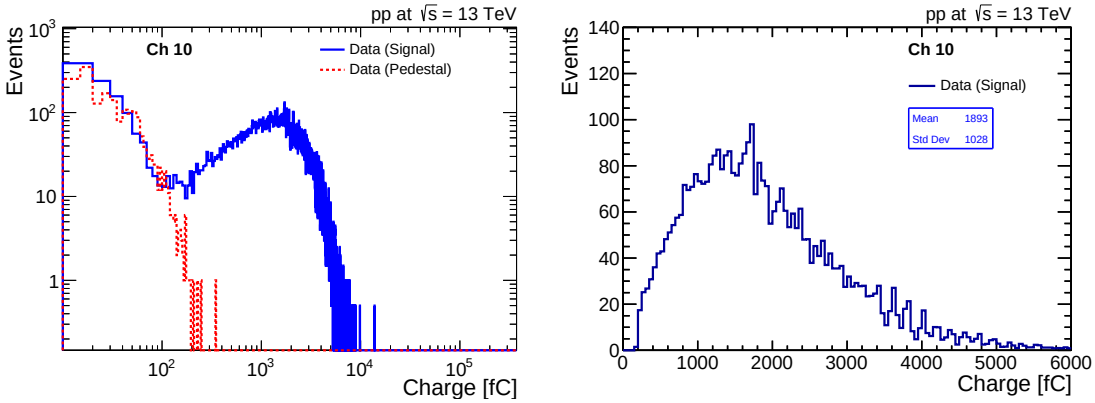

Figure 15. Left: Charge distribution of non-interacting events from circulating beam runs (red) and the FCD charge distribution of colliding beam events from (blue). Horizontal log scale used to make the separation of circulating and colliding beams more visible. Right: The FCD charge distribution after the residual background elimination using non-interacting events.

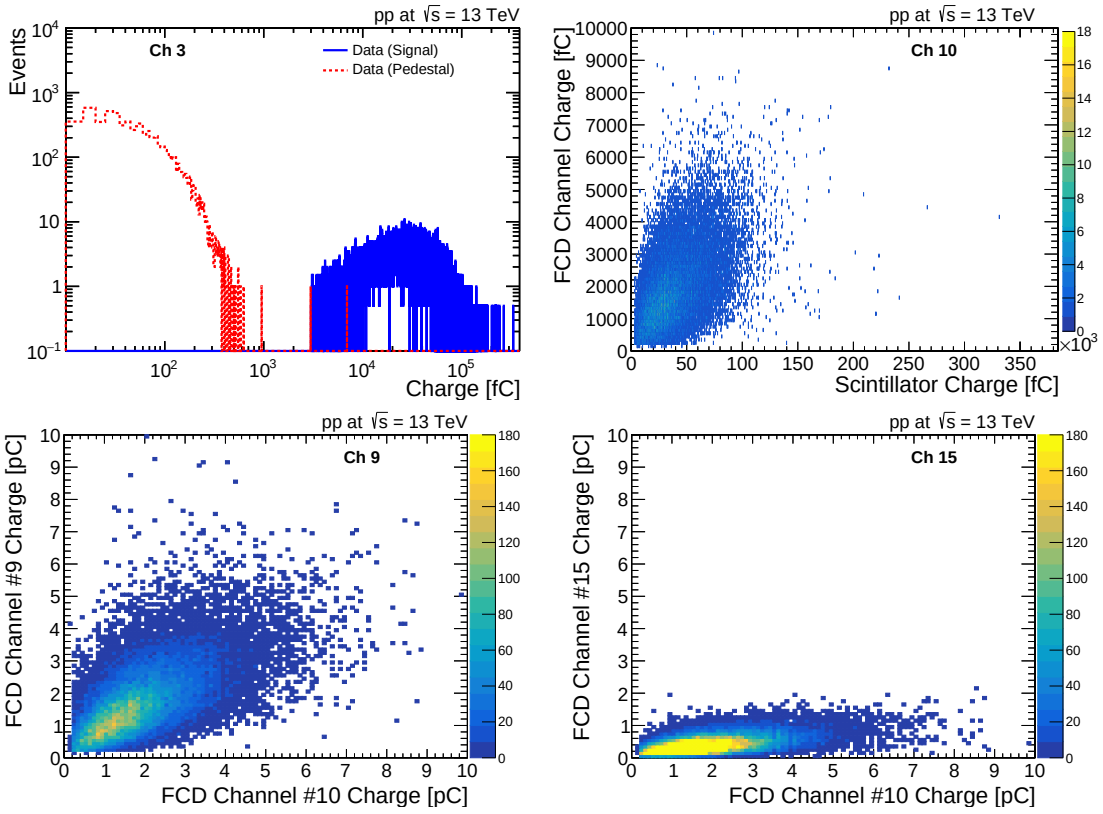

Figure 16. Left: The trigger scintillator charge distribution (blue); in red the background from non-interacting beams events. Right: The charge correlation between the triggering scintillator and one of the FCD channel. The lower plots show the charge correlations between the different channels of the FCD

are given in Fig. 3.4 where errors are less than the symbols' size. The four groups of points represent the Q2 columns, in similar pairs (e.g. C1 and C3, C2 and C4). The mean values of

the charge distributions for the FCD channels are scattered around an average level of about 1 pC and spread from 0.5 pC to 1.5 pC approximately. This is the range of mean charges measured for some QUARTIC Q2 channels in the test beam with 180 GeV/c negative π (taking into account the different signal attenuation of the SiPMs during test beam and LHC 13 TeV collisions). Numerical estimates and MC simulations agree with these results once significant effects of light attenuation in the bulk of quartz bars, and losses at the bar surface and quartz bar to SiPM coupling are realistically taken into account.

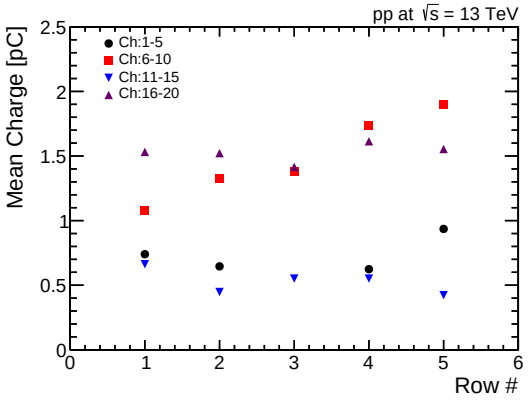

Figure 17. The mean values of the charge distributions for the FCD channels; note that Channel 3 is the trigger scintillator and is not shown here.

The TDC distribution for one of the FCD channel is shown in the Figure 18 (left). The values of mean and STD of the corresponding TDC distribution are also given in the plot. The mean values and STD of the TDC time distributions for all the FCD channels are shown in Fig. 18 (right). The mean values of TDC times show a flat distribution. Note that Channel 3 is the trigger scintillator and not included in the figure.

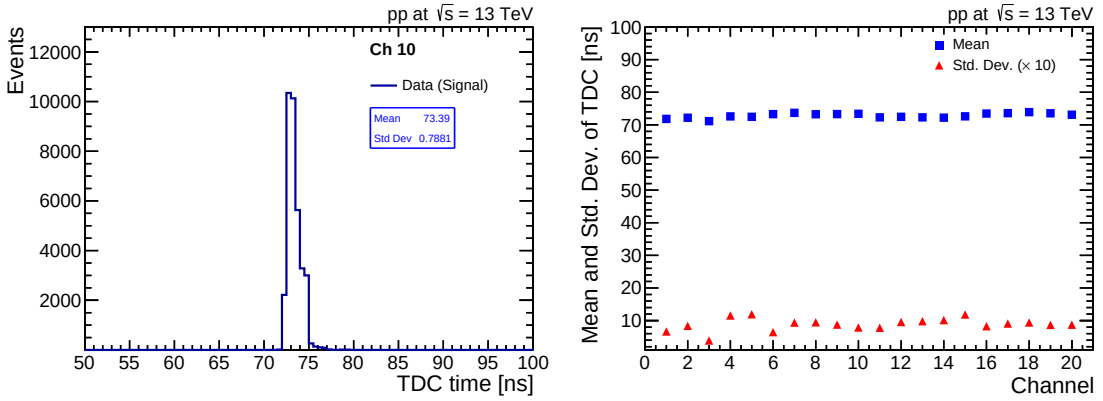

Figure 18. (Left)The TDC distribution for one the FCD channel. Events are selected above the threshold chosen for charge spectra; (Right) Mean values and STD of the TDC time distributions for all the FCD channels.

4 Comparison of results with expectations and MC simulations

The mean charge measured for the FCD-PD Q2 channels in the H8 test beam with 180 GeV/c π^- and at 13 TeV pp collisions is in a range of some pC that may be reasonably supposed to originate from Minimum Ionizing Particle (MIP) hitting one of the quartz bars. The average signals from a Q2 SiPM would therefore correspond to about 10^7 electrons. For a SiPM gain G $\approx 10^6$ and PDE $\approx$ 35 % (averaged from 350 to 650 nm) an effective number of 30 photons reaching the SiPM window would be estimated. This is between 20 and 60 times less photons then the expected photons created in accordance to the radiator bar lengths. In fact the timing precision requirement imposes strict Total Internal Reflection (TIR) transmission of Cherenkov photons along the quartz bars. Use of light confining methods (reflective wrapping, etc.) is excluded and perfect surface quality of the quartz bars has to be achieved at production stage, with a roughness RMS ≈ 0.1 μm and at assembly (minimal contact with the bars' surfaces). Usually optical methods are applied to check the surface conditions of quartz samples [26] (e.g. Interferometry); however the studies refer to very small surfaces of few samples. A recently proposed method [27] is quite interesting as it permits (in some cases) to characterize fused silica bars' surface quality with a β-source, possibly in-situ and over the whole surface of the bar. Their results could suggest that the quartz bar surfaces might have reflectivity some percent below 1 globally, leading to high losses due to multiple bouncing on the surfaces of the quartz bars. Furthermore, the edges of the bars may present incomplete the TIR, if any, for a sizeable width. The close packing of the bars in the Q2 assembly may represent an additional complication.

Numerical estimates and MC simulations have been performed for the Cherenkov photon production and transport in the quartz bars. Results on the GEANT4 simulation of the production and transmission of Cherenkov photons in quartz bars of various dimensions are obtained. The simulations are extended to study more subtle effects of light attenuation in the bulk of quartz bars, and losses at the bar surface, as well as incomplete transmission at the entrance window of the photodetector that need to be properly parametrised to be simulated. For the numerical estimate and simulations of the response of a QUARTIC module, the geometries of the quartz bars are given in Table 6.

Table 6. The geometry of the quartz bars and number of photons estimated

	Q2 channel.				**R1**	**R2**	**L**	**R1+L**	**R2+L**	$\mathbf{N}_{ph1}$	$\mathbf{N}_{ph2}$
Raws	**C1**	**C3**	**C2**	**C4**	**(mm)**	**(mm)**	**(mm)**	**(mm)**	**(mm)**	**(300-650 nm)**	**(300-650 nm)**
1	1	11	6	16	63.0	58.0	71.2	134.2	129.2	1990 ± 40	1830 ± 40
2	2	12	7	17	53.0	48.0	68.1	121.1	116.1	1680 ± 40	1520 ± 40
3	3	13	8	18	43.0	38.0	65.0	108.0	103.0	1360 ± 30	1200 ± 30
4	4	14	9	19	33.0	28.0	61.9	94.9	89.9	1040 ± 30	890 ± 30
5	5	15	10	20	23.0	18.0	58.8	81.8	76.8	730 ± 20	570 ± 20

The QUARTIC-Q2 assembly (FCD) is composed of 20 L-bars, having ten different radiator R lengths, forming two groups of almost equivalent pairs (R1 and R2); L are the lengths of the light-guide parts. The number of Cherenkov photons per unit length and wavelength interval is estimated from Eq. 2.1; for a single-charged relativistic ($\beta \approx 1$) particle (MIP), the typical photon

yield for quartz (n ≈ 1.46), in the SiPM sensitivity range ($\lambda \approx 350$ - 650 nm), could be $Y_c \approx 30$ N_{ph} mm. Numerical estimates of the produced Cherenkov photons, should be corrected for the principal transmission losses to obtain the number of photons N_{ph}, reaching the SiPM window, according to an approximate formula:

$$N_{ph} \approx (Y_c \times R) \times \Gamma^{\nu} \times exp[-\gamma \times (R + L)/L_{abs}] \tag{4.1}$$

where L_{abs} is the absorption length in quartz; γ is an expansion coefficient of the photons' path in the bar, due to their bouncing on the faces of the bar by TIR, ν is the number of bounces and Γ is the reflection efficiency at each bounce. With respect to Eq. 4.1, simulations provide more precise information and allow to describe in a correctly random way the most important losses in the L-bars. The L-bars are represented in GEANT4 as in Fig. 19, where a typical QUARTIC L-bar is hit by a particle coming from the left (blue line), along the R-segment axis and emits Cherenkov photons according to Eq. 2.1 along its path, at an angle θ_c with respect to its trajectory; the photons' paths are shown with green lines, which are in part collected in the L-Bar and transported to the SiPM front face, and in part are lost by absorption in the bulk material, in part escape from the L-bar surfaces; these different cases are summarized in Table 7.

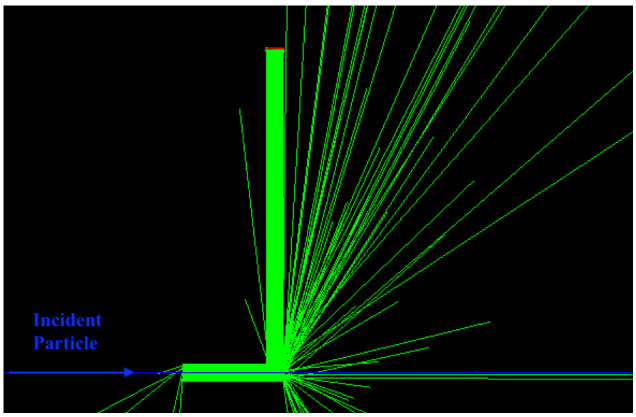

Figure 19. Full simulation of (charged) particle hitting a quartz L-bar

Table 7. The number of photons estimated at SiPM with different conditions

QUARTIC Q2					N_{ph} Created (300-750nm)		N_{ph} Reach to SiPM (300-750nm)		N_{ph} Converted at SiPM (300-750nm)	
Raw Number	Column Number				Assuming $Y_C \times R$		L_{abs} from Table 1 $\Gamma = 1, CC = 1$		PDE Gain = 10^6	
#	**C1**	**C3**	**C2**	**C4**	**C1-C3**	**C2-C4**	**C1-C3**	**C2-C4**	**C1-C3**	**C2-C4**
1	1	11	6	16	1990 ± 40	1830 ± 40	1340 ± 30	1350 ± 30	450 ± 20	450 ± 20
2	2	12	7	17	1680 ± 40	1520 ± 40	1320 ± 30	1360 ± 30	440 ± 20	460 ± 20
3	3	13	8	18	1360 ± 30	1200 ± 30	1360 ± 30	1350 ± 30	450 ± 20	440 ± 20
4	4	14	9	19	1040 ± 30	890 ± 30	1380 ± 30	1180 ± 30	450 ± 20	400 ± 20
5	5	15	10	20	730 ± 20	570 ± 20	960 ± 30	780 ± 30	340 ± 20	300 ± 10

The Table 7 displays the situation when the produced photons are lost only by absorption in the quartz bar (L_abs is given in Table 1), the surface quality of the bar is perfect ($\Gamma = 1$) and the

contact of the bar end with the SiPM window is also perfect Contact Coefficient (CC = 1). The bulk absorption produces an average loss of photons of about 25 %, and surface losses, due to impacts of photons with the quartz bar surface at angles larger than the critical angle, are less than 10 %. The photons reaching the SiPM window and developing avalanches in the detector are about 25 % of the total number of produced photons in the interval (300 - 750 nm). The collected charge at SiPM output would be of about 40 pC which is about 25 times more then the measured charge both at H8 and LHC.

Introducing a non-perfect reflectively at the quartz bar surface (Γ = 0.98), and a contact coefficient CC= 0.75 at the interface of the bar end and the SiPM window, the amount of photons transmitted through the bar and collected by the SiPM are reduced to levels compatible with the measured charges (Table 8). The increased losses at the surface have two very important effects: reducing the difference of photons from different bars, and emitting a large number of photons outside the bar, with randomized angles, which would make easier their trapping in another bar, thus increasing the number of cross-talk in Q2. Now the losses in transmission through the L-bars are almost 77 %, and the number of photons reaching the SiPM is about 100. It is clear that this drastic reduction in photons reaching the SiPM allows to bring the GEANT4 simulations in agreement with the charges measured at H8 and LHC. A reflectivity of 98 % is still acceptable and correspond to a good surface quality; the contact of the bar end with the SiPM window should be improved via optical cement or highly transparent silicone pads. The average gain of this type of SiPMs is 10^6, for an over-voltage of 3V, but each individual SiPM has slightly different gain, which would also influence the response of the Q2 channels.

Table 8. The number of photons estimated at SiPM with non perfect conditions

QUARTIC Q2					N_{ph} Transmitted (300-750nm)		N_{ph} Reach to SiPM (300-750nm)		N_{ph} Converted at SiPM (300-750nm)	
Raw Number	Columns Number				L_{abs} from Table 1 Γ = 0.98		Bar-SiPM CC=0.75		PDE Gain= 0.5×10^6	
#	**C1**	**C3**	**C2**	**C4**	**C1-C3**	**C2-C4**	**C1-C3**	**C2-C4**	**C1-C3**	**C2-C4**
1	1	11	6	16	460 ± 20	430 ± 20	100 ± 10	100 ± 10	30 ± 10	30 ± 10
2	2	12	7	17	480 ± 20	420 ± 20	100 ± 10	100 ± 10	40 ± 10	40 ± 10
3	3	13	8	18	460 ± 20	400 ± 20	100 ± 10	100 ± 10	30 ± 10	40 ± 10
4	4	14	9	19	390 ± 20	390 ± 20	100 ± 10	100 ± 10	40 ± 10	40 ± 10
5	5	15	10	20	330 ± 20	370 ± 20	100 ± 10	90 ± 10	30 ± 10	30 ± 10

In conclusion, while a direct estimate of the Cherenkov photons produced in a spectral interval compatible with SiPM sensitivity, corrected for simple absorption in the quartz L-bar, would give a relatively large amount of photons reaching the SiPM window and producing avalanches in the SiPM, compatibility with the much smaller measured signals in test beam and at LHC, requires substantial photon losses at the quartz bar surface, and not complete optical contact between the bar end and the SiPM window.

5 Radiation Effects

During the period between TS2 and TS3, when the FCD module was in place on the CASTOR table, the LHC collected about 14 fb^{-1} integrated luminosity at the IP5 (CMS) collision region (Fig. 20, left). The radiation levels behind the HF calorimeters, about 15 m from IP5, are quite high (see Fig. 20, center and right). From these plots it is possible to estimate the dose and neutron flux at the position of the FCD module.

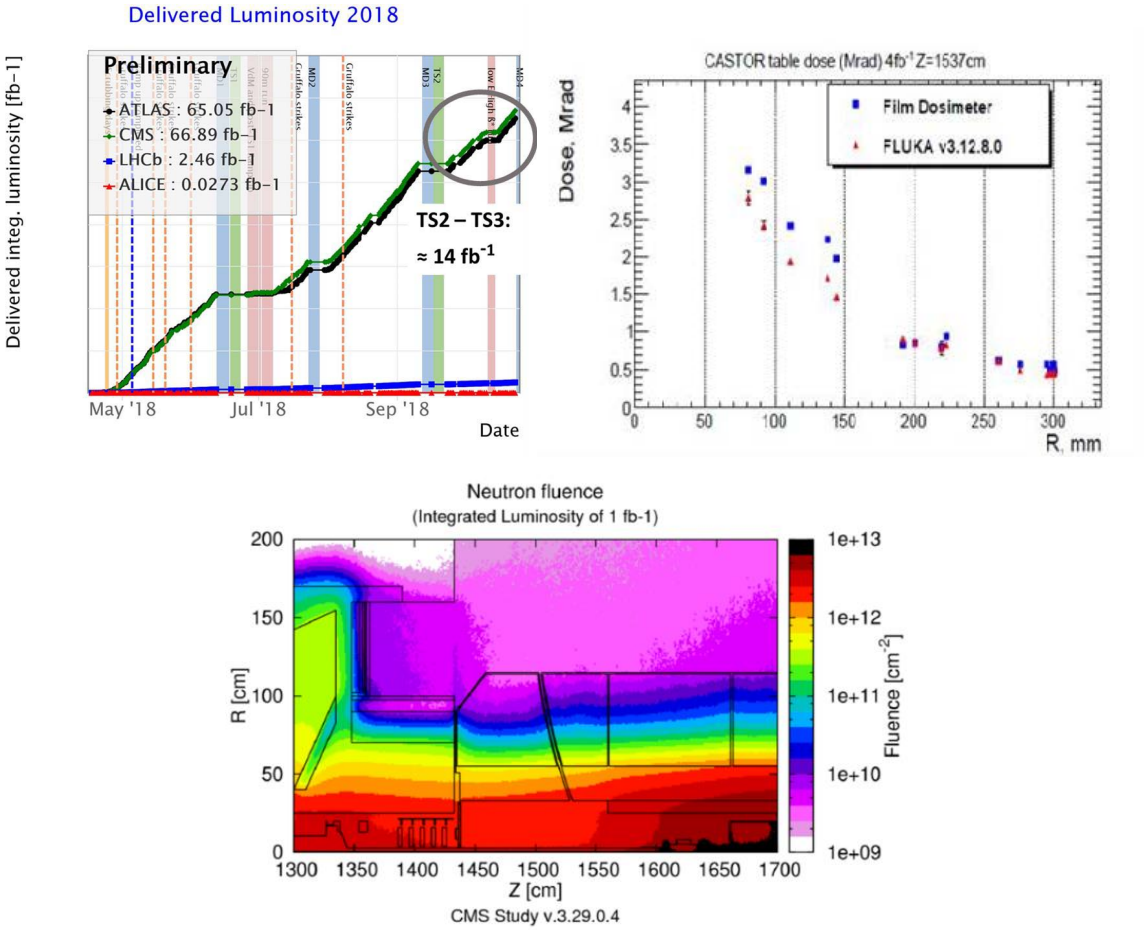

Figure 20. (Left) The pp integrated luminosity delivered in 2018 at LHC. (Right)The dose at CASTOR table, for 4 fb^{-1} (Bottom) The map of neutron flux for 1 fb^{-1}

5.1 Dose received by the SiPM

The FCD module is based on quartz L-bars (expected to resist very high radiation levels) and SiPMs, in principle more sensitive to radiation, in particular neutrons. The FCD channels are equipped with MPPC S-12572-050-P (Hamamatsu) and the trigger scintillator with one MPPC S10931-050P. According to the configuration of the FCD module, the Q2 SiPM were located at about 150 mm distance from the beam line, and the trigger scintillator + SiPM were centered at 96 mm. These kind of MPPC, and other similar ones have been tested up to 10^{13} n/cm^2 [28, 29], showing significant radiation effects (i.e. dark current increase) starting around 10^{12} n/cm^2.

The doses received by the FCD SiPMs can be estimated as:

- At r≈ 90 mm, 14 $fb^{-1}\times$ 0.75 Mrad/fb^{-1} ≈ 10.5 Mrad
- At r≈ 150 mm: 14 $fb^{-1}\times$ 0.5 Mrad/fb^{-1} ≈ 7.0 Mrad
- Neutron fluence: $14fb^{-1} \times 5 \times 10^{12}(n/cm^2)/fb^{-1} \approx 7x10^{13}$ n/cm^2

At these levels of radiation, in particular neutron flux, there is a serious risk of radiation damage both for the SiPM and other electrical components of the bias voltage distribution card. Radiation could have two main effects on electronics: single event effects (SEE) and total ionising dose (TID) effects. Single event effects are due to highly energetic particles, which can cause bit flips in digital circuits or voltage spikes in analogue circuits. The total ionizing dose is an accumulating effect, of the dose rate and the total time a circuit is exposed to radiation [30, 31].

5.2 SiPM Defect characterization

Various techniques used for the microscopic investigation of defects in silicon, such as Deep-Level Transient Spectroscopy (DLTS), Thermally Stimulated Current (TSC) techniques and IR-absorption spectroscopy may be applied to SiPM, with some specific difficulties, due to their large capacitance and high dopant concentration [32] [4].

IR-spectroscopy measurements on SiPMs are not reported in the literature, which could be an alternative way to characterize radiation defects. Another qualitative way to visualize the effect of radiation damage is to observe the light emission in the dark from a SiPM biased above breakdown. This is based on the phenomenon that every Geiger discharge emits a certain number of optical and IR photons produced in the high field region. DLTS measurements were performed[5] on the SiPM, which was used to read out the trigger scintillator during the period in CMS. Comparisons of irradiated and non-irradiated SiPM (Fig. 21) clearly shows the effect of irradiation (estimated $\Phi_{eq} \approx 3 \times 10^{13}$ n/cm^{-2}).

6 Summary and Conclusions

At LHC IP5, housing the CMS and TOTEM experiments, among various forward detectors using Cherenkov light-emitting quartz radiators and photodetectors, principally in view of the superior radiation resistance of quartz, a special category of detectors (QUARTIC) were intended to measure the time-of-flight of very forward protons scattered at the interaction point IP5 and reaching the Roman Pots of TOTEM-PPS in the LHC tunnel. For the QUARTIC module, a collaboration of CERN, IHEP and FNAL was involved in the development and the production of the detectors. The QUARTIC quartz L-bar configuration allowed to assemble a 2D detector, edge-less and radiation hard, with photo-detectors sufficiently far from the beam region, to suffer less radiation damage.

[4] Non-irradiated SiPM could have a doping concentration of the order of $N_d \leq 10^{16}$ cm^{-3}, and assuming a DLTS sensitivity limit of about $N_{trap} = 10^{-4}\times N_d$, a trap concentration of $N_{trap} > 10^{12}$ cm^{-3} is too high with respect to the expected trap concentration from radiation damage, at least for low and medium fluences up to $\Phi_{eq} \approx 10^{12}$ cm^{-2}. For higher fluences the trap concentration may reach a measurable level.

[5] courtesy of Omer Goksel Erbas

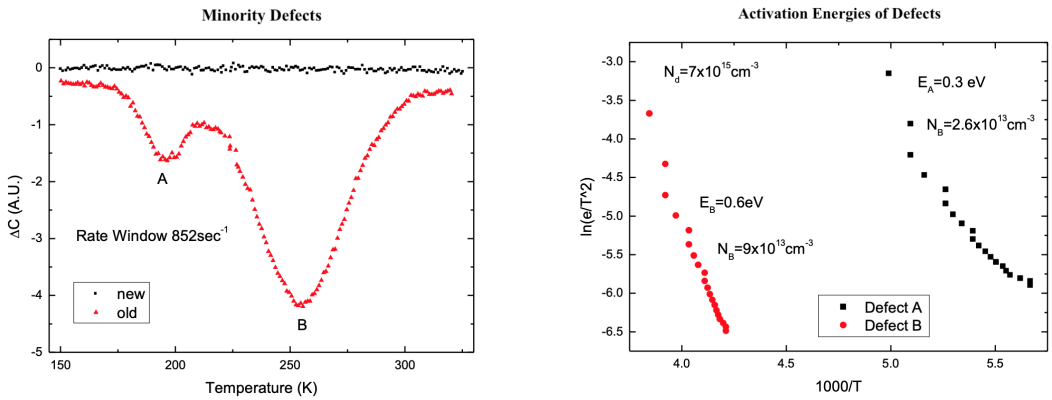

Figure 21. DLTS measurements on two SiPM (irradiated/non-irradiated) for the FCD trigger scintillation

The conceptual properties of these devices were tested at FNAL as prototypes with a limited number of quartz L-bars and MCP-PMT or SiPM photodetectors.

The production of two QUARTIC detectors with 20 L-bars (+ SiPM) each was completed in 2015 and tested at CERN. One critical point of the project was the requirement of a perfect optical quality of the fused silica L-bars produced in single pieces, in order to guarantee the best transmission of Cherenkov photons from the radiator segment to the photodetector. The 2015 CERN test beam results of modules provided timing resolutions less precise than the 2012 FNAL prototypes. One goal of the measurements described here was to investigate in more detail the behaviour of the QUARTIC modules, and possibly to demonstrate the advantage of this technology at very high pseudorapidity (generically FCD).

The Q1 and Q2 modules were checked; Q1 had some non-functioning channels and therefore, we concentrated on the Q2 module, which was first refurbished at IPM-Tehran and equipped with a bias voltage distribution card; back at CERN the module was tested with a LED and radioactive sources, mounted on a mechanical support for installation at the H8 test beam and at the CMS Castor Table on the HFM platform. After having tested the module at H8, reading four channels at a time with a DSO, full readout with the HFM QIE-10 system was tested at B904 and transferred to CMS UXC5 in September 2018. During TS2, 36 M events of 13 TeV pp collision at different run conditions were collected and analyzed to study the behaviour of the FCD channels, described here.

The charge distributions in individual channels present practically the same mean values for both the H8 test beam (180 GeV/c π) and at CMS IP5 (13 TeV pp) measuring and spread varying from 0.5 pC to 1.5 pC approximately, with RMS from 0.2 pC to 0.3 pC. Timing measurements at H8 (with DSO) show typical resolutions $\sigma_t \approx 200$ ps with QIE-10, the TDC bin width is 0.5 ns, and the time distributions have RMS of about 0.7 ns. Both the charge measurements and the timing resolutions indicate important photon losses, producing relatively small signals from the SiPM, with the consequence of modest time resolution.

The results from 2018, in two totally different environments, agree rather consistently with the main conclusions from the 2015 QUARTIC test beams. The radiation effects on the FCD module

during the LHC data taking were rather high which causing the module failure after few days of operation. This could be due to damage on the SiPM themselves and/or on the components of the bias voltage distribution card.

At TS3, the module was removed from UXC5 and transported, under RP supervision, to B226 controlled storage room, where it was possible to perform a survey of operational conditions of the Q2 module, in comparison with the (non irradiated) Q1 module. With a spare Bias Voltage distribution card, it was possible to operate all the Q2 channels again; the problem at the level of the irradiated card could be traced back to some of the components, including a Zener diode (BV stabilization), a LED (BV connection display) and a chip controlling the humidity and temperature. The Q2 SiPM were responding to LED (and radioactive source) but with an increased baseline shift, which is a sign of dark current (and radiation damage). Even more significant, the behaviour of the trigger scintillator and SiPM in front of the Q2 L-bars which still respond to radioactive source and LED respectively, but with some instabilities and much increased dark current. A DLTS study of the irradiated (scintillator) SiPM shows presence of changed density and energy of defects. Similar analysis for the Q2 SiPM was not possible up to now due to the residual activity of the Q2 module.

Despite accidental interruption, the FCD test at UXC5 has provided sufficient information to further the development of quartz detectors. With respect to the L-bar configuration, straight bars will be investigated in more details; such configurations could be adapted to calorimetry with superior timing. Concerning the photodetectors, MCP-PMTs appear to provide better time resolution and are built with multi-channel output. Radiation resistance remains a crucial requirement, for each element of the devices under study.

The tests performed at H8 and UXC5 despite different environment and operating conditions have various points in common and give a number of important lessons for future studies and/or design generic prototypes based on similar technologies:

- Despite their flexibility and high degree of hardware/software built-in equipment and applications, DSO instruments (Agilent, WR-LeCroy) have a limited number of channels, which may be useful in laboratory activities, but definitely need multi-channel, wide bandwidth, large storage, programmable waveform digitizers for beam acquisition; data storage and backup need large portable disk memories.

- A continuously (self-)calibrating time reference counter (TRC; $\sigma_t \approx 10$ ps or less) should replace standalone reference timing counters which are occasionally calibrated, under the assumption that their (excellent) resolution would not change with time, temperature, or other conditions.

- Simple, fast, moderate (space) resolution tracking system coupled with DUT and TRC systems.

- LED/LD light pulsers with (few) ps precision (and stability) should be available for field (frequent) calibrations.

- One serious problem appears to be the step from single (or few-) channel(s) prototypes to multi-channel systems, preserving the excellent properties of the former, and taking advantage of the redundancy of the latter.

Acknowledgments

We would like to acknowledge M. G. Albrow for proposing the QUARTIC scheme, and providing to us the two modules; S. Los has designed and built the SiPM readout. We thank A. Ball, P. De Barbaro, J. Dittmann, Y. Onel, P. Rumerio and W. Zeuner for encouragement and advice. We are grateful to M. Bozzo and M. Berretti for their help and advice in using the H8 beam. We congratulate the Accelerator Division personnel for their excellent operation of the CERN machines, in particular SPS and North Area beam lines for the H8 data taking and the LHC collider during the last part of the 13 TeV pp run in 2018. A. Apyan, A. Kaminsky, R. Kellogg, E. Laird, M. Toms have helped us with integrating a FCD read out into the HCAL Data Acquisition system and with data taking; G. Antchev, I. Atanassov, F. Bonini, B. Dinger, X. Pons, Yu.V. Mikhailov and S. Jamili have assisted us in various phases of the commissioning and operation of the FCD module. We gratefully thank A. Heering for the SiPM used with the defining scintillator and information on SiPM radiation damage. F. De Guio, D. R.-H. Yu and S. Abdullin have helped in integrating FCD in the CMS data acquisition and in the analysis. This study was partly funded by the Scientific Research Projects Coordination Unit of Istanbul University Project number FUA-2018-32919. Lastly, we would like thank to PPS Technical and Management Coordination and CMS HCAL Technical and Management Coordination for their full support.

References

[1] M. Akatsu, Y. Enari, K. Hayasaka, T. Hokuue, T. Iijima, K. Inami et al., *Mcp-pmt timing property for single photons*, *Nuclear Instruments and Methods in Physics Research Section A: Accelerators, Spectrometers, Detectors and Associated Equipment* **528** (2004) 763 – 775.

[2] K. Inami, N. Kishimoto, Y. Enari, M. Nagamine and T. Ohshima, *A 5 ps tof-counter with an mcp–pmt*, *Nuclear Instruments and Methods in Physics Research Section A: Accelerators, Spectrometers, Detectors and Associated Equipment* **560** (2006) 303 – 308.

[3] I. Dumanoglu, N. Akchurin, U. Akgun, S. Ayan, P. Bruecken, E. Eskut et al., *Radiation-hardness studies of high oh content quartz fibres irradiated with 500mev electrons*, *Nuclear Instruments and Methods in Physics Research Section A: Accelerators, Spectrometers, Detectors and Associated Equipment* **490** (2002) 444 – 455.

[4] K. Cankoçak, M. Bakırcı, S. Çerçi, E. Gülmez, J. Merlo, Y. Onel et al., *Radiation-hardness measurements of high oh- content quartz fibres irradiated with 24gev protons up to 1.25grad*, *Nuclear Instruments and Methods in Physics Research Section A: Accelerators, Spectrometers, Detectors and Associated Equipment* **585** (2008) 20 – 27.

[5] A. Penzo, *Calorimetry and cherenkov radiation*, *Nuclear Instruments and Methods in Physics Research Section A: Accelerators, Spectrometers, Detectors and Associated Equipment* **595** (2008) 264 – 266.

[6] A. Penzo, Y. Onel and the CMS Collaboration, *The CMS-HF quartz fiber calorimeters*, *Journal of Physics: Conference Series* **160** (2009) 012014.

[7] E. Norbeck, Y. Onel, E. Gladysz-Dziadus, A. D. Panagiotou and P. Katsas, *Exotic physics at the LHC with CASTOR in CMS*, *Int. J. Mod. Phys. E* **16** (2007) 2451–2456.

[8] O. A. Grachov, M. J. Murray, A. S. Ayan, P. Debbins, E. Norbeck, Y. Onel et al., *Status of zero degree calorimeter for CMS experiment*, *AIP Conf. Proc.* **867** (2006) 258–265, [nucl-ex/0608052].

[9] A. G Anelli, P. Aspell, V. Avati, M. G. Bagliesi, V. Berardi, M. Berretti et al., *The TOTEM experiment at the CERN large hadron collider*, *Journal of Instrumentation* **3** (2008) S08007–S08007.

[10] M. Albrow, P. Collins and A. Penzo, *Forward Shower Counters for diffractive physics at the LHC*, *Int. J. Mod. Phys.* **A29** (2014) 1446018.

[11] M. Albrow, M. Arneodo, V. Avati, J. Baechler, N. Cartiglia, M. Deile et al., *CMS-TOTEM Precision Proton Spectrometer*, Tech. Rep. CERN-LHCC-2014-021. TOTEM-TDR-003. CMS-TDR-13, 2014.

[12] "Hamamatsu webpage." `http://www.hamamatsu.com/`.

[13] S. Grinstein, *The atlas forward proton detector (afp)*, *Nuclear and Particle Physics Proceedings* **273-275** (2016) 1180 – 1184.

[14] M. G. Albrow, H. Kim, S. Los, M. Mazzillo, E. Ramberg, A. Ronzhin et al., *Quartz Cherenkov Counters for Fast Timing: QUARTIC*, *JINST* **7** (2012) P10027, [1207.7248].

[15] M. Oriunno, M. Battistin, E. David, P. Guglielmini, C. Joram, E. Radermacher et al., *Design and prototype studies of the totem roman pot detectors*, *Nuclear Instruments and Methods in Physics Research Section A: Accelerators, Spectrometers, Detectors and Associated Equipment* **581** (2007) 499 – 503.

[16] J. Vavra, D. W. G. S. Leith, B. Ratcliff, E. Ramberg, M. Albrow, A. Ronzhin et al., *Beam test of a time-of-flight detector prototype*, *Nuclear Instruments and Methods in Physics Research Section A - accelerators Spectrometers Detectors and Associated Equipment - NUCL INSTRUM METH PHYS RES A* **606** (2009) 404–410.

[17] A. Ronzhin, M. Albrow, M. Demarteau, S. Los, S. Malik, A. Pronko et al., *Development of a 10ps level time of flight system in the fermilab test beam facility*, *Nuclear Instruments and Methods in Physics Research Section A: Accelerators, Spectrometers, Detectors and Associated Equipment* **623** (2010) 931 – 941.

[18] M. Gallinaro and M. Khakzad, *Timing detectors for PPS: status and plans*, *PPS General Meeting, CMS Week* (2015) .

[19] "Agilent webpage." `https://www.agilent.com`.

[20] GEANT4 collaboration, S. Agostinelli et al., *GEANT4: A Simulation toolkit*, *Nucl. Instrum. Meth.* **A506** (2003) 250–303.

[21] G. Blaj, C. J. Kenney, A. Dragone, G. Carini, S. Herrmann, P. Hart et al., *Optimal pulse processing, pile-up decomposition, and applications of silicon drift detectors at lcls*, *IEEE Transactions on Nuclear Science* **64** (2017) 2854–2868.

[22] E. Gatti and V. Svelto, *Theory of time resolution in scintillation counters*, *Nuclear Instruments and Methods* **4** (1959) 189 – 201.

[23] T. Zimmerman and M. Sarraj, *A second generation charge integrator and encoder asic*, *IEEE Transactions on Nuclear Science* **43** (1996) 1683–1688.

[24] T. Zimmerman and J. R. Hoff, *The design of a charge-integrating modified floating-point adc chip*, *IEEE Journal of Solid-State Circuits* **39** (2004) 895–905.

[25] J. Mans, J. Anderson, B. Dahmes, P. de Barbaro, J. Freeman, T. Grassi et al., *CMS Technical Design Report for the Phase 1 Upgrade of the Hadron Calorimeter*, Tech. Rep. CERN-LHCC-2012-015. CMS-TDR-10, 2012.

[26] D. Malacara, *Optical Shop Testing*. John Wiley & Sons, 3rd ed., 2007.

[27] A. Natochii et al., *Characterisation of the fused silica surface quality with a β-source*, *Nucl. Instrum. Meth. A* **910** (2018) 15–21.

[28] B. Biró, G. David, A. Fenyvesi, J. S. Haggerty, J. Kierstead, E. J. Mannel et al., *A comparison of the effects of neutron and gamma radiation in silicon photomultipliers*, *IEEE Transactions on Nuclear Science* **66** (2019) 1833–1839.

[29] A. Heering, Y. Musienko, R. Ruchti, M. Wayne, A. Karneyeu and V. Postoev, *Effects of very high radiation on sipms*, *Nuclear Instruments and Methods in Physics Research Section A: Accelerators, Spectrometers, Detectors and Associated Equipment* **824** (2016) 111 – 114.

[30] M. Brugger, M. Calviani, R. Garcia Alia, J. Mekki and G. Spiezia, *R2E – EXPERIENCE AND OUTLOOK*, in *Proceedings, 4th Evian Workshop on LHC beam operation: Evian Les Bains, France, December 17-20, 2012*, (Geneva), pp. 13–18, CERN, 2012.

[31] G. Spiezia et al., *The LHC Radiation Monitoring System - RadMon*, *PoS* **RD11** (2011) 024.

[32] E. Garutti and Y. Musienko, *Radiation damage of sipms*, *Nuclear Instruments and Methods in Physics Research Section A: Accelerators, Spectrometers, Detectors and Associated Equipment* **926** (2019) 69 – 84.